LA-UR -82-3339

Conf-821089--4

Los Alamos National Laboratory is operated by the University of California for the United States Department of Energy under contract W-7405-ENG-36

LA-UR--82-3339

DE83 003059

TITLE: SUPRATHERMAL-ELECTRON GENERATION, TRANSPORT, AND DEPOSITION IN CO_2-LASER-IRRADIATED TARGETS

AUTHOR(S): Allan Bauer, R. Goldman, R. Kristal, M. A. Yates, M. Mueller, F. Begay, D. van Hulsteyn, K. Mit[illegible]. Eckhart, H. Gona, E. Stover, J. Brackbill, and D. Fo

SUBMITTED TO: 6th International Workshop on Laser Interaction and Related Plasma Phenomena, Monterey, CA, October 25-29, 1982.

Los Alamos National Laboratory
Los Alamos, New Mexico 87545

SUPRATHERMAL-ELECTRON GENERATION, TRANSPORT, AND DEPOSITION IN CO_2-LASER-IRRADIATED TARGETS

Allan Hauer, R. Goldman, R. Kristal, M. A. Yates, M. Mueller, F. Begay, D. van Hulsteyn, K. Mitchell, J. Kephart, H. Oona, E. Stover, J. Brackbill, and D. Forslund

Los Alamos National Laboratory
University of California
Los Alamos, NM

ABSTRACT

In CO_2-laser interaction with matter most of the absorbed energy is initially channeled into a hot-electron distribution. Im many cases, resonance absorption is thought to be the dominant mechanism producing this distribution. Stimulated scattering may also play an important role.

In the coronal region of the laser plasma, hot electrons suffer losses that fall into two basic categories. First, hot electron energy is used in the sheath to accelerate fast ions. In some cases this can be a very-efficient process. This is an important interaction, since some ICF concepts use energetic ions as the drive mechanism. The other coronal-loss mechanism is the loss of energy to cold electrons through the drawing of a return current. Some aspects of the absorption and coronal loss processes will be illustrated by experiments on laser-irradiated shells.

Experiments on both axial and lateral energy transport and deposition in spherical targets are described. A variety of diagnostics have been used to measure hot-electron transport and deposition including bremsstrahlung and inner-shell radiation and soft-x-ray temperature measurements. Self-generated electric and magnetic fields play an important role in the transport and deposition of the hot electrons. In some cases distinct patterns of surface deposition consistent with magnetic-field configurations have been observed.

I. INTRODUCTION

In this paper we report progress toward understanding the absorption and subsequent partitioning of CO_2 laser energy incident on solid targets. The efficiency of absorption of laser light and its subsequent partitioning into useful forms such as fast ion energy is, of course, crucial to the evaluation of any particular laser for its ICF potential.

We presently believe that all of the absorbed CO_2 laser energy must initially reside in a hot (> 50 keV at $I > 10^{15}$ W/cm^2) electron distribution. We thus deal in Section I with the hot electron generation (CO_2 absorption) mechanisms. In Section II, we discuss the results of absorption measurements at moderate to high intensity. After absorption, we proceed to the next most direct interaction, the exchange of hot electron energy with fast ions. In Section III, fast ion measurements are discusssed. The role of magnetic fields in fast ion generation is discussed in relation to experimental results. Finally, we deal in Section IV with the transport and deposition of the remaining hot electrons and the picture of overall energy balance. Once again self generated magnetic fields play an important role. X-ray imaging indicated distinct signatures of magnetically mediated transport patterns.

Some of the important elements of recent progress are:

1. A new perspective on absorption (and hot electron generation) at high intensity (> 10^{15} W/cm^2).

2. Measurement of high energy conversion to fast ions in a variety of target configurations and the effect of magnetic fields on this conversion.

3. Observation of non diffusive lateral energy transport due to self generated magnetic fields.

4. Consistent overall energy balance/partitioning in high intensity experiments.

II. LASER ABSORPTION AND HOT ELECTRON GENERATION

The primary diagnostic of absorbed laser energy (on the Helios 8 beam CO_2 laser system) is an array of plasma/x ray calorimeters. These devices record the total ion and x-ray energy produced by the target interaction (while rejecting scattered CO_2 light). These calorimeters have been calibrated, both electrically and with accelerator produced ion beams.[1]

A substantial number of these devices are placed in strategic locations so that angular variation of the ion blowoff can be determined. Filtered counterparts of the total energy calorimeters are used to assess the energy in fast ions.

In Table I, we show the results of a typical absorption study. Shells 300 μm in diameter coated with various materials were irradiated at surface focus ($I \simeq 10^{16}$ W/cm^2). The gold shells were also irradiated at defocused conditions ($I \sim 5 \times 10^{15}$ W/cm^2). There is no variation in total absorption with target material. There was, however, a considerable variation in absorption with focal conditions (and correspondingly with flux density).

TABLE I

Absorption for 300 μm targets is high, independent of target material.

	TARGET (300 μm DIAMETER)	ABSORPTION
SURFACE FOCUS	GMB	58%
	GMB WITH 20 μm CH	58%
	GMB WITH 3 μm Au	57%
DEFOCUSED 500 μm	GMB WITH 3 μm Au	36%

GMB = GLASS MICROBALLOON

The high absorption at high intensity is quite encouraging for ICF applications. It is possible that this high absorption may be explained by a recent calculation of resonance absorption at high intensity. This picture predicts deformation and rippling of the critical surface that results in enhanced absorption and higher hot electron temperature.

With appropriate underdense plasma conditions, Raman scattering may compete with critical surface absorption. Experiments are planned in the near future to better define the underdense plasma conditions in typical CO_2 target configurations. It is possible that the lower absorption at defocused conditions may also be due to an enhancement of side scatter.

In Fig. 1, we show the scaling of absorption with focal conditions for two diameters of shell targets. For the defocus conditions shown in Fig. 1, the f/2.4 focused laser beams are translated the indicated distances beyond surface focus. There is some evidence that the difference in total absorption for the very large targets is due to poorer angular coverage by the calorimeter array (ions emitted back toward the focusing optics and not collected by calorimeters). The pronounced variation in absorption with focal conditions, however, remains.

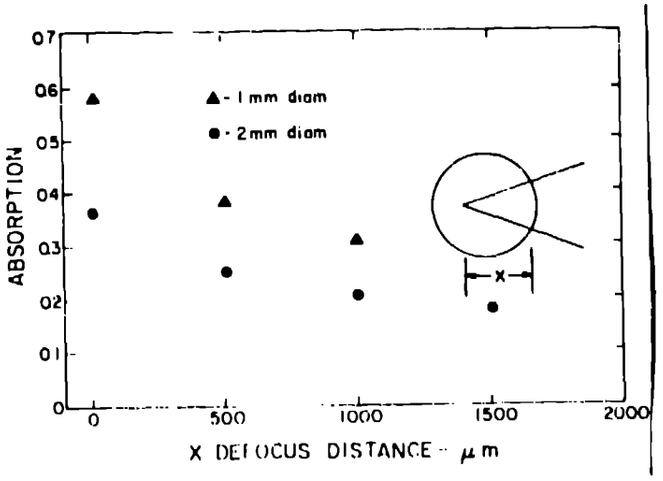

Fig. 1. CO_2 laser absorption as a function of focal conditions.

The temperature of the hot electron spectrum generated by the absorption processes is also of great importance to the determination of target coupling efficiency and preheat. The primary diagnostic of T_{hot} is the hard x-ray spectrum.[2] The hard x-ray bremsstrahlung spectrum provides a "transported" indicator of T_{hot}, since most of these long mean free path electrons radiate at significant distances from their point of origin near the critical surface (stopping in the high density regions of the target). The source hot electron temperature (implied by the bremsstrahlung measurement) is usually inferred from the results of hydrodynamic or particle code simulations. These simulations are often run so as to match the observed hard x-ray spectrum. The hot electron source temperature needed for this replication is then determined. This operation, for example, takes into account the energy loss to fast ions and the effect of this loss on the hard x-ray spectrum.

In CO_2 interaction experiments, the hot electron temperature observed in the above way seem generally higher than can be explained by the usual picture of resonance absorption.[3] In Fig. 2, we show experimental measurements of T_{hot} (x-ray) as a function of laser intensity on target. Calculations of T_{hot} by the usual resonance absorption formulation would imply a lower T_{hot} than observed. In addition, the scaling with

intensity in the region > 10^{15} W/cm^2 is steeper than anticipated (between $I^{0.4}$ and $I^{0.5}$). The $I^{0.5}$ line in Fig. 2 seems to represent the best fit to scaling in the region of I > 10^{15} W/cm^2. It is drawn through the entire range for reference only and is not meant to imply a constant slope throughout the intensity range. There are several possible explanations for higher T_{hots}:

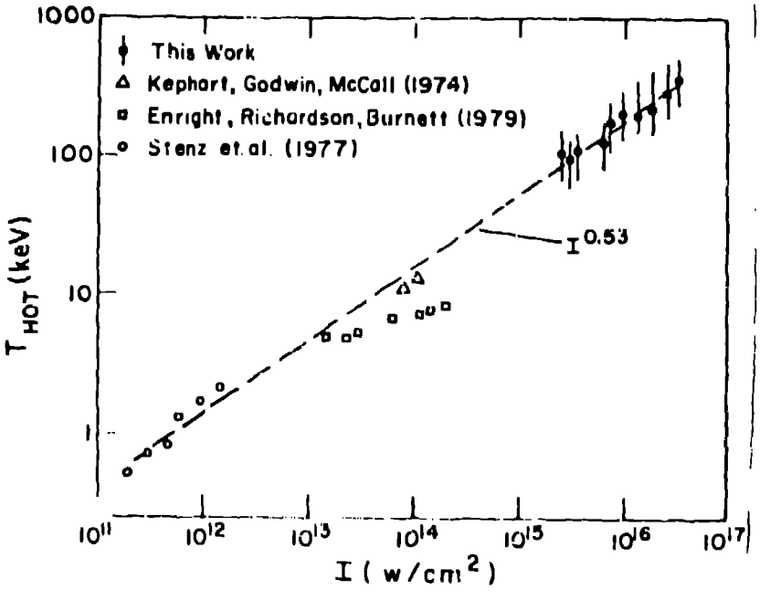

Fig. 2. T_{HOT} (x-ray) as a function of laser irradiance

1. T_{cold} may be higher than previously thought.

Results from recent particle simulations (the new resonance absorption calculation mentioned above) show higher T_{hot}. The higher T_{Hot} may be due in part to an enhancement of T_{cold} due to an electron two-stream instability between the inward streaming hot electrons and outward flowing cold electrons. The scaling of T_{hot} should be: $T_H \propto (I\lambda^2 T_c)^{0.3-0.5}$. A higher T_c could thus possibly account for observations.

2. Raman scattering remains a strong possibility even though optical measurements made at Los Alamos indicate very little $\omega_0/2$ or $3\omega_0/2$ light emitted from the target plasma. Measurements are needed to better characterize underdense plasma conditions (addressing the Raman question) and T_c. It must thus be recognized that the high absorption observed at high intensity may also be accompanied by very high temperature. This may have positive implications for fast ion generation, but be negative from the point of view of preheat.

III. FAST ION MEASUREMENT AND THEORY

The calorimeters described in Section II are also used to measure the energy in fast ion expansion. To perform this measurement they are filtered with thin metal foils (which typically pass 100 keV protons). As with total energy measurements, the angular distribution of the fast ions is determined by an array of calorimeters (in this case filtered).

In Table II we show the fracton of absorbed energy in fast ions measured on the same targets as in Table I. Large fast ion fractions are observed for tight surface focus conditions. The total conversion of laser energy to fast ion energy approached 40%. The fraction is reduced at defocused conditions. This reduction may be due in part to a lowering of the energy of some of the ions below the calorimeter filter cutoff. Very little variation in fast ion fraction with the wall thickness of the shell is measured.

TABLE II

Fast Ion Fraction For
Various Shell Targets.

	Target (300 μm Diameter)	Fast Ion Fraction (of Absorption)
SURFACE FOCUS	GMB	65%
	GMB WITH 20 μm CH	58%
	GMB WITH 3 μm Au	62%
DEFOCUSED 500 μm	GMB WITH 3 μm Au	43%

The mechanism for the generation of fast ions is intimately tied to self generated magnetic fields. Recent calculations[4] have revealed many interesting aspects of these fields. In some cases, hot electrons are confined to the coronal region of the plasma for much longer times than they would be without the fields. This implies a longer period of interaction with the plasma sheath and higher conversion to fast ions.

Some interesting aspects of fast ion conversion are illustrated by studies of the irradiation of shells of varying thickness. In the simple model to fast ion acceleration, hot

electrons make one or more bounces off the sheath giving up $\sim 2\sqrt{(Z/A)(m_e/m_p)}$ on each encounter.[5] As the thickness of the target increases, the energy loss in dense material goes up and fewer bounces would be expected to occur. From this picture one might expect higher conversion in thin targets. Filtered plasma calorimeter experiments, however, show little variation with thickness.

Magnetic field modeling shows that for thick targets the hot electrons are confined by the field to the coronal region causing a significant interchange with ions, while reducing the energy loss in the dense material.

For thinner layers of material, the multiple bounce model may be more appropriate. In this case, electrons can penetrate the dense material of the target and more uniformly heat it. This tends to break up the magnetic field pattern permitting the simple bounces off the sheath to occur. In the section below, we will present evidence for the breakup of the magnetic field patterns in thin targets.

Let us consider a simple example of a 1 μm wall gold shell irradiated so that the hot electron temperature is about 120 keV. The loss/bounce from the sheath is $\sim 2\sqrt{(Z/A)(m_e/m_p)} \sim 0.045$ Accounting for collisional loss in dense material, sheath velocity, and core decoupling, about 8 bounces would occur. This would give a fast ion fraction of 0.36 and about 0.40 is observed. In the thin walled case, the simple picture is thus numerically consistent with observations.

In summary, the conversion of laser energy to fast ion expansion can be a very efficient process. CO_2 laser accelerated ions may prove very useful in testing ion driven ICF concepts.[6]

IV. HOT ELECTRON TRANSPORT AND DEPOSITION AND ENERGY BALANCE

Hot electrons generated near the critical surface seem to transport and deposit their energy in a rather complicated way. In most cases the transport is strongly affected by self generated electric and magnetic fields. These fields affect not only the spatial distribution of energy, but the overall energy balance (such as the partitioning of energy into fast ions). We deal first with deposition and overall energy balance and then with some characteristics of the spatial distribution of deposition.

Hot electron transport and deposition have been experimentally diagnosed with x-ray imaging and spectral measurements and with charged particle spectral and calorimetric measurements.

The hard x-ray spectrum is measured with a 10 channel foil filtered detector array.[2] This instrument covers the spectral range from 30 keV to 1 MeV.

The hard x-ray (bremsstrahlung) temperature and yield are taken as indicators of hot electron energy that is collisionally deposited. It was shown by Bethe and Heitler[7] that the ratio of collisional to radiative losses is given by:

$$\frac{(dE/dx)RAD}{(dE/dx)COLL} = \frac{EZ}{800}, \qquad (1)$$

where E is in units of MeV. This general proportionalty between collisional and radiative losses is confirmed by measurements on targets that are thick to the electron energies involved. Integrating over a Maxwellian distributon gives an approximate relationship between the ratio of hard x-ray yield to T_{hot} and collisionally deposited electron energy:

$$E_{COLL} = \frac{Y}{T_H} \; 1/\{10^{-6} \; Z(1 + n/2)\}, \qquad (2)$$

where n is the dimensionality of the Maxwellian distribution and T_H = hot electron temperature. This is the same formula that is empirically derived from thick target bremsstrahlung experiments.[8]

A more careful analysis of bremsstrahlung using recently available cross sections[9] is underway. The preliminary indication is that Eq. (2) gives an overestimate of the collisional energy loss.

Bremsstrahlung does not measure non-collisional losses. Stopping of fast electrons by loss to collective oscillations could be very important.[10]

In the first three columns of Table III we show the results of hard x-ray measurements on a laser irradiated gold shell (the values tabulated are averages over 6 laser shots).

TABLE III

Wall Thickness (μm)	T_{hot} (keV)	Collisional Deposition Implied By Hard X-Rays (J)	T Soft X-Rays eV	Soft X-Rays (50 eV-2 keV) Yield (J)
~ 10.0	200	352 (0.075)	135	20 (0.047)

The third column in Table III uses the simple approximate formula given in Eq. (2) and assumes a 3 dimensional Maxwellian. Also shown in this column, in parenthesis, is the collisional deposition as a fraction of incident laser energy.

Hard x-ray emission samples electron deposition in deep layers of the shell. Soft emission, on the other hand, samples deposition in a thin layer near the surface of the target. The thickness of this layer is approximately one absorption length or around one micron in the case of gold.[11] In the last two columns of Table III, we show the results of soft x-ray measurements (covering the spectral range 50 eV to . keV). The temperature is obtained by fitting a blackbody spectrum to the outputs from a 7 channel (broadband foil filter) soft x-ray detector. These temperatures and the integrated x-ray energy can be used to estimate the total deposition in the shell by comparisons with overall hydro modeling of the interaction.

Combining the x-ray measurements with calorimeter results, a picture of the overall energy balance begins to emerge. This balance is indicated in Fig. 3. About 675 J is not directly accounted for experimentally for the same case as that illustrated in Table III.

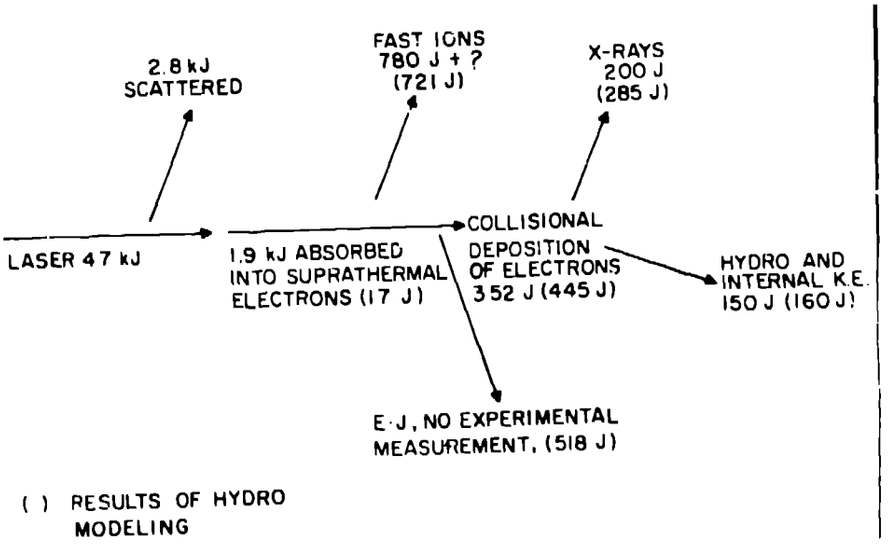

Fig. 3.
Energy balance in CO_2 laser irradiated shell.

Figure 3 also contains the results of hydro code simulation of the same (average) laser shot. The hydro simulation results in parenthesis are compared with experimental values averaged over 6 laser shots. The simulations were performed by adjusting the hot electron distribution so that the bremsstrahlung spectrum matches that observed in the experiment. The agreement between theory and experiment is reasonably good. More refined experiments and simulations are, however, required to reduce the descrepancy in deposited (and potentially useful) energy.

There are several possibilities to account for the energy not accounted for experimentally: (a) fast ions not measured by the calorimeters (e.g., protons below 100 keV), (b) a lower component (or components) of T_{hot} that collisionally deposit such that the corresponding bremsstrahlung is not observed, and (c) return current loss of hot electron energy to the cold distribution ($E \cdot J$ Losses).

Experiments have recently been undertaken to help answer the question of a lower component (or components) of T_{hot}. A crystal spectrograph as been constructed that covers the range of 4-23 keV. A spectrum produced by this device is shown in Fig. 4. This shot represented about 5 kJ of CO_2 laser light incident on a gold shell (2000 μm diam, 10 μm thick wall). The 20 keV distribution has an upper bound of 2 J of total energy.

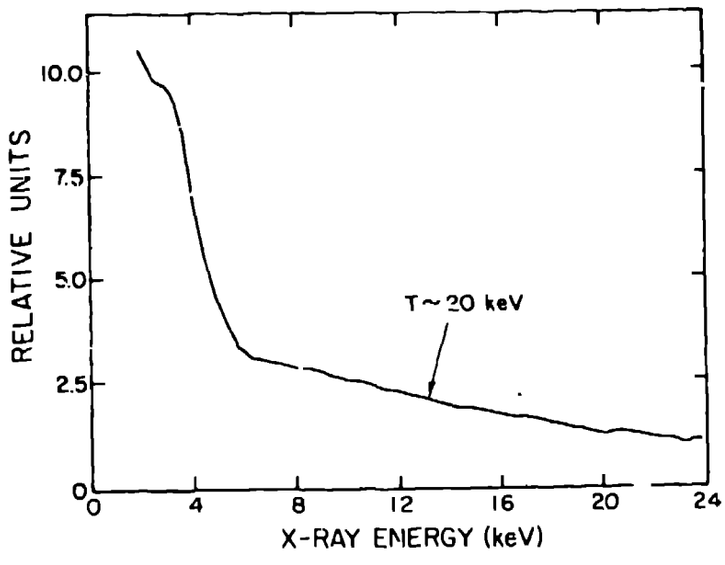

Fig. 4. 4-26 keV X-ray spectrum from a CO_2 laser irradated gold shell.

Here one cannot use the simple formula given in Eq. (2) for the interpretation of collisional deposition. This is because at these lower energies the absorption of the radiation and severe alteration of the electron spectrum in thin layers necessitate fairly complex modeling as described below. Our approach toward

this very preliminary information has been to attempt to reconcile the data with the results of hydro code simulations. Thus far, only a small amount of the absorbed energy can be placed in the ~ 20 keV distribution and still reproduce adequately the hard and soft x-ray measurements (such as those described above).

In the remainder of this section we deal with some of the spatial characteristics of hot electron transport and deposition.

In addition to fast ion production, self generated magnetic fields have important effects on energy transport. The most prominently observable effect is the non diffusive nature of lateral transport.

The recently developed 2-D, implicit electromagnetic simulation code VENUS calculates the self consistent magnetic fields and the resulting energy tranport. One of the results is that many of the hot electrons remain confined to the region around the focal spot. The remainder are transported considerable distances from the spot. One such calculational result is indicated in Fig. 5.

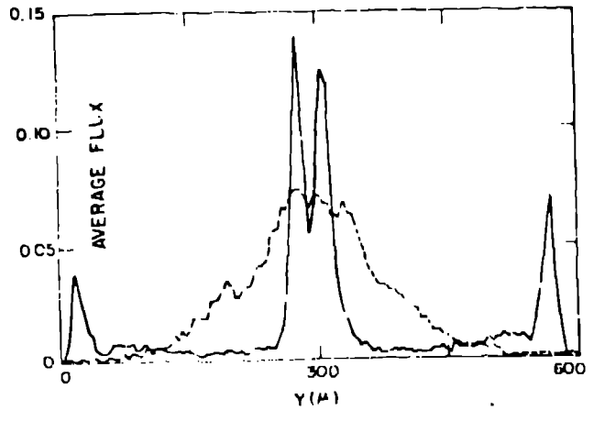

Fig. 5. Integrated energy transport across the back of a foil as a function of position on the foil. The dashed line responds to $B = 0$ and the solid line to $B \neq 0$.

Lateral transport across the back of a laser irradiated foil is calculated with and without magnetic fields. In Fig. 6, we show experimental evidence of the same phenomena. Two laser spots incident on a gold disk are separated by 1 mm. The electron deposition pattern is diagnosed by 1-2 keV x-ray imaging. The observed deposition region corresponds to the interference pattern predicted by the 2-D transport model.

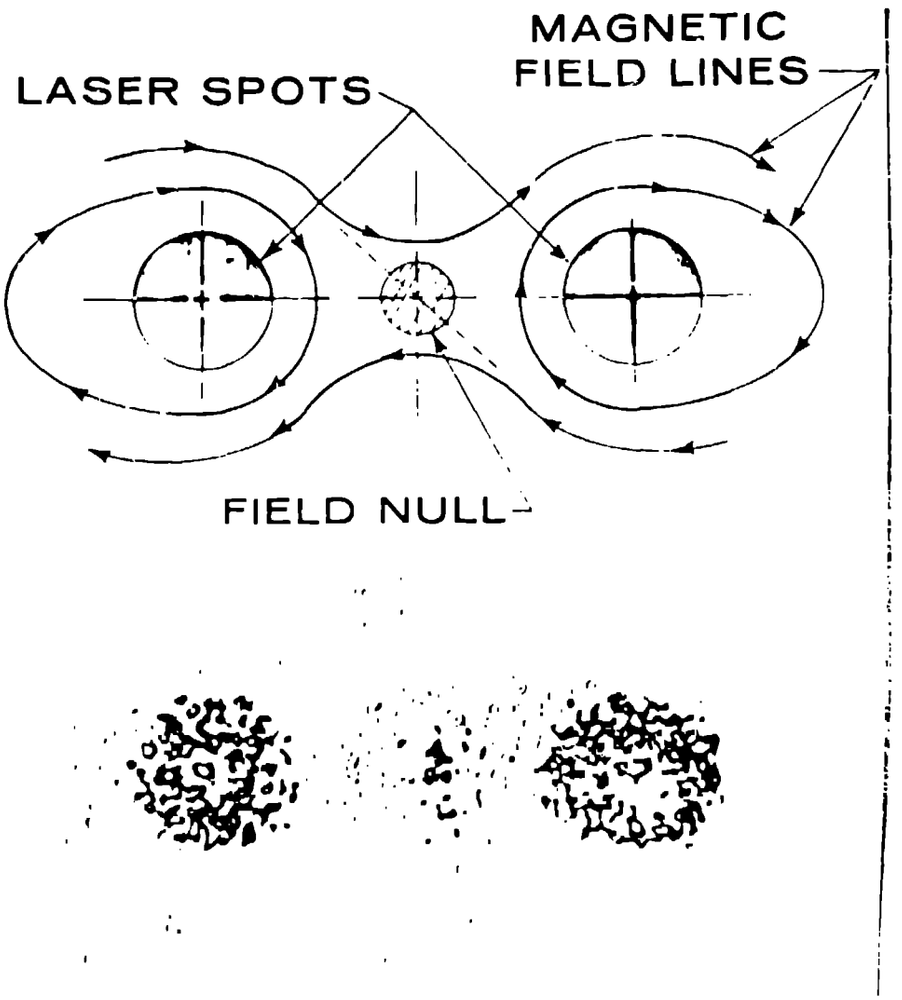

Fig. 6.
1-2 keV x-ray image produced by two laser irradiation spots separated by 1 mm.

In Fig. 7, we show the lateral deposition pattern on shells of varying thickness. As discussed in the section on fast ions, the magnetic field pattern is disrupted in the tain walled case. This gives further confirmation to the overall picture of energy transport and fast ion production.

Experiments have been recently undertaken to measure axial transport using K_α radiation. The targets are composed of shells of K_α radiating materials, such as copper and nickel. Prelminary results from these experiments indicate a higher deposition in the outer layers than would be predicted using the hard x-ray measurements as the normalization. This may indicate supra-thermal flux limitation.

Fig. 7.
1-2 keV x-ray images of the laser irradiation of gold shells of varying wall thickness.

CONCLUSIONS

Calorimeteric measurements have demonstrated high CO_2 laser absorption at high intensities. This absorption and its corresponding T_{hot} is consistent with recent calculations of resonant absorption.

High efficiency of conversion of laser energy to energetic ions has been measured. New modeling techniques involving self consisten B fields calculate correctly many aspects of hot electron coupling to fast ions.

Strong experimental evidence for non-diffusive lateral transport of hot electron energy has been presented.

X-Ray and calorimetric measurements are a good overall picture of fast electron energy partitioning. In many respects, these measurements agree with hydrodynamic simulations.

ACKNOWLEDGEMENT.

The work of the Helios laser and target fabrication teams has made possible the large number of laser shots on which these studies have been based.

The authors would like to acknowledge the valuable comments of Philip Goldstone on all aspects of this work.

REFERENCES

1. J. F. Kephart, A. H. Williams, Los Alamos National Laboratory Internal Memo. See also Proceedings of 12th Anomalous Absorption Conf., Santa Fe, NM, May 10–13, 1982.

2. W. Priedhorsky, D. Lier, R. Day, and D. Gerke, Phys. Rev. Lett. 47 (23) p. 1661 (1981).

3. D. W. Forslund, J. M. Kindel, and K. Lee, Phys. Rev. Lett. 39 (5) p. 284 (1977).

4. D. W. Forslund and J. U. Brackbill, Phys. Rev. Lett. 48 (23), p. 1614 (1982).

5. R. L. Morse and C. W. Nielson, Phys. Fluids 16 (6), p. 909 (1973).

6. C. W. Barnes, et al., Bull. Am. Phys. Soc. 27 (8) II, p. 1067 (1982).

7. H. Bethe and W. Heitler, Proc. Roy. Soc. Lond. Ser. A 146 (83) (1934).

8. A. H. Compton, S. K. Allison, X-Rays in Theory and Experiment (D. van Nostrand 1935).

9. J. Feng and P. H. Pratt, "Parameterization of the Bremsstrahlung Spectrum," Contract Report to the Department of Energy (Univ. of Pittsburgh Report PITT 266, July 1981).

10. A. Bauer and F. Burns, Proc. on XII International Conf. on the Physics of Electronic and Atomic Collisions, Gatlinburg, Tennessee, 15-21 July 1981 (North Holland 1982).

11. B. Henke, et al., "Atomic and Nuclear Data Tables," Vol. 27 (1) (January 1982) p. 1.